Civil Engineering Dimension
https://ced.petra.ac.id

# Investigation on the Structural Behaviour of GFRP Laminated BFRC Beams

**Arulanandam, P.M.[1]*, Shimpi, V.[2], and Eswari[3]**
[1] Asisstant Professor, Department of Civil Engineering, Mohamed Sathak A.J. College of Engineering, Chennai 603103, INDIA
[2] Project Engineer, VMS Consultant Pvt.Ltd., Mumbai 400021, INDIA
[3] Associate Professor, Department of Civil Engineering, Puducherry Technological University, Pondicherry 605014, INDIA

DOI: https://doi.org/10.9744/ced.27.2.123-134

***Article Info:***
Submitted: Feb 25, 2025
Reviewed: Mar 12, 2025
Accepted: May 13, 2025

***Keywords***:
ANSYS,
BFRC,
crack pattern,
GFRP,
load-deflection response.

***Corresponding Author:***
**Arulanandam, P.M.**
Asisstant Professor, Department of Civil Engineering, Mohamed Sathak A.J. College of Engineering, Chennai 603103, INDIA
Email: civil.preethymary@msajce.edu.in

**Abstract**

This study attempts to investigate the performance of the reinforced concrete beam by using basalt fibre reinforced concrete (BFRC) and glass fibre reinforced polymer (GFRC) as external strengthening. For this purpose, four beams with different strengthening were cast and tested under four-point bending tests. The performance of the beams was compared in terms of mid-point deflection, flexural strength, ductility and failure modes. Additionally, finite element models of the beams have been developed to simulate the behaviour of the strengthened beams. Subsequently, the finite element results were compared with the experimental results and were found to be in good agreement. Finally, the experimental testing and numerical results showed that the flexure capacity of the reinforced concrete beams was enhanced for GFRP strengthening and reduction in the deflection of the beams was observed for BFRC.



## INTRODUCTION

The need for strengthening reinforced concrete (RC) structures is growing due to increased load demands, functional changes, material degradation, and design flaws. Externally bonded fibre-reinforced polymer (FRP) sheets, strips, or plates offer an effective solution, enhancing efficiency, reliability, and cost-effectiveness [1]. Common FRP types include carbon (CFRP) [2], glass (GFRP), and aramid (AFRP) fibre-reinforced polymers [3]. GFRP, known for its high strength, temperature resistance, and affordability, is particularly favored in Asia over carbon fibre composites [4]. However, FRP applications in seismic zones remain limited due to complex resistance mechanisms [5].

While FRP strengthening increases load capacity, it often reduces ductility. Studies show FRP-strengthened beams can achieve a 16% higher ultimate load but 54% less deflection than unstrengthen beams [6]. To improve ductility, short discrete fibres—such as steel or synthetic fibres—are incorporated into concrete [7]. Steel fibres enhance compressive strength but are prone to corrosion and reduce workability [8] while glass fibres are sensitive to alkaline conditions [9]. Carbon fibres offer stiffness but are costly and anisotropic [10].

Basalt fibre (BF), a new alternative, is extracted from melted basalt rock, offering superior mechanical properties at a lower cost than glass or carbon fibres [11]. Its tensile strength surpasses E-glass fibres and significantly exceeds steel fibres. Studies confirm FRP composites effectively enhance flexural capacity [12]. Retrofitting RC beams with CFRP and GFRP significantly improves load-bearing performance, with numerical and experimental results aligning closely.

**Note** : Discussion is expected before November, 1st 2025, and will be published in the "Civil Engineering Dimension", volume 28, number 1, March 2026.
**ISSN** : 1410-9530 print / 1979-570X online
**Published by** : **Petra Christian University**

Kachlakev and McCurry [13] retrofitted four-shear deficient RC beams with CFRP and GFRP composites. The study reported that FRP composites for structural strengthening provides significant static capacity compared to un-strengthened sections. Chiew et al. [14] investigated the flexural behaviour of RC beams strengthened with GFRP laminates experimentally and numerically. The study reported that both flexural strength and stiffness of RC beams were enhanced by such a bonding technique. Further, the numerical results agreed well with the experimental results. Hence, in the present study, the influence of key parametres relating to the strength, deformation, and ductility of the externally bonded GFRP laminated BFRC beams by both experimental and numerical methods were investigated. The numerical study was performed using the ANSYS [15] software, to conduct simulations and analyses. The numerical results in terms of the load-carrying capacity, deflection and load versus mid-span deflection curves are compared with obtained experimental results.

## MATERIAL PROPERTIES

### Basalt Fibre Reinforced Concrete (BFRC)

The BFRC in this study comprised ordinary Portland cement, local river sand, water, and 1% basalt fibres by volume. Basalt fibres, with a length of 18 mm and a diametre of 1 μm (aspect ratio of 18), exhibit a tensile strength of 2.9–3.1 GPa and an elastic modulus of 85–87 GPa, with a density of 2.65 g/cm³. The BFRC mix proportions are detailed in Table 1. Compressive tests on 150 mm cube specimens yielded an average compressive strength of 30.15 MPa, while split tensile tests on 100 mm × 200 mm cylinder specimens recorded an average strength of 3.50 MPa. Figure 1 presents the basalt fibre properties, and Figure 2 illustrates the test setup and stress-strain curve for compression.


**Figure 1.** Photographic View of Basalt Fibre [16]

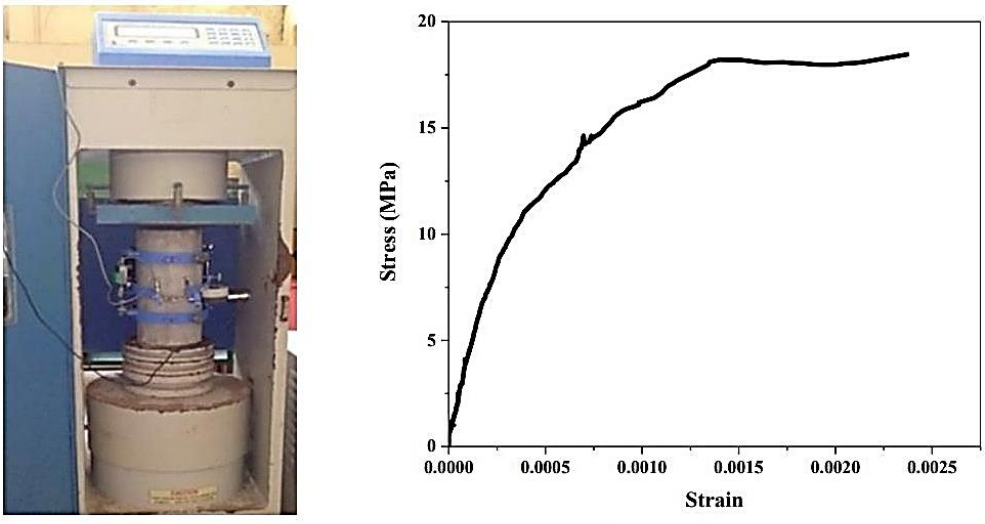


(a) Test setup (b) Stress-strain curve

**Figure 2.** Stress-strain Curve of BFRC

**Table 1.** Mix Proportion Adopted in the Study.

| Materials | Cement (kg/m³) | Sand (kg/m³) | Coarse aggregate (kg/m³) | Water (kg/m³) | Fibre (kg/m³) |
|---|---|---|---|---|---|
| BFRC | 350 | 720 | 1180 | 160 | 26.7 |
| C | 350 | 720 | 1180 | 160 | - |

## Concrete and Steel Reinforcement

The concrete used in this study was designed to have a strength grade of C25. Compression and split tensile tests were performed on the concrete, using cubes and cylinder specimens. The average compressive and split tensile strength of the concrete was found to be 28.23 MPa and 3.20 MPa, respectively. The mix proportions of concrete are presented in Table 1. Further, the mechanical properties of the steel reinforcement used in this study are listed in Table 2.

**Table 2.** Mechanical Properties of Steel Reinforcement.

| Diameter (mm) | Yield Strength ($fy$) (MPa) | Ultimate Strength ($fu$) (MPa) | Young's Modulus ($E$) (GPa) |
|---|---|---|---|
| 10 | 415 | 620 | 200 |
| 8 | 415 | 620 | 200 |

## GFRP Laminate

A commercially available EL005 uni-directional E-Glass fabric was used as the strengthening agent. It is particularly suitable for applications where high stiffness is required in one direction. A photographic view of the unidirectional glass fabric is shown in Figure 3. The GFRP laminate used in this study consists of a single layer with a thickness of 5 mm. It exhibits an ultimate stress of 503.2 MPa and a modulus of elasticity of 1603.5 MPa. Additionally, the Poisson's ratio for the GFRP laminate is 0.38.

**Figure 3.** Photographic View of The Unidirectional Glass Fabric

## Beam Details

Four steel reinforced beam specimens with different specifications were cast and tested. The geometry and reinforcement details of the beam specimens are shown in Figure 4. The main flexural reinforcement for the beams consisted of two 10 mm deformed bars and two 8 mm deformed bars, as hanger bars. The shear reinforcement for the beams were provided with 8 mm diametre deformed bar spaced at 150 mm c/c. The GFRP laminate of 5 mm thick was externally bonded at the soffit of the RC and BFRC beams. The beams are casted based the mix design method adopted as per Indian code. The casted RC and BFRC beams were shown in Figure 5.

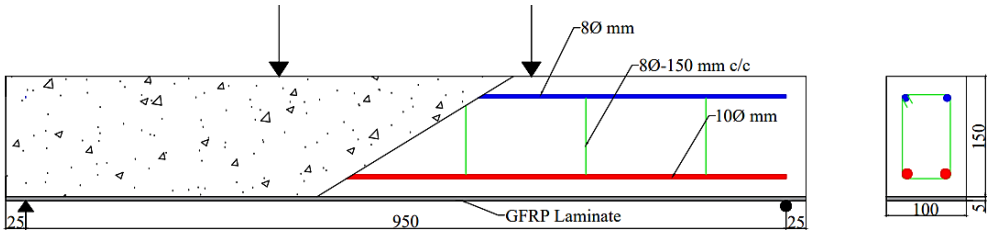


**Figure 4.** Geometry and Reinforcement Details Beam Specimen

(a) RC Beams (b) BFRC Beams

**Figure 5.** Casted Beam Specimens

## Strengthening of Beams

The strengthening technique employed in this study is adopted from the ACI. After casting and normal curing of the beams for 28 days, the beams were strengthened by external bonding of unidirectional glass fabric, using epoxy resin as the adhesive, on the tension face of the beam. To ensure proper bonding between concrete and laminate, the beam surface was prepared using mechanical grinding and then the surface was cleaned with the help of a brush to remove all fine particles from the prepared surface. The resin was applied uniformly to the prepared surface. The reinforcing fibres were gently pressed into the uncured resin and the resin was squeezed through the weaving of the fabric with a roller. The different stages of strengthening of the beam are shown in Figure 6.

(a) Grinding of Concrete Surface

(b) Application of Epoxy Resin

(c) Laying GFRP Layer

(d) Applying Resin and Removal of Air Bubbles Simultaneously

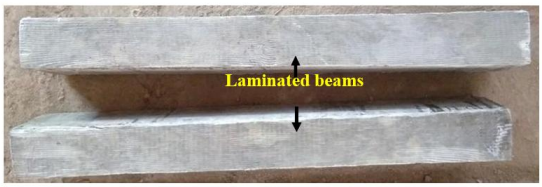


(e) Laminated Beams

**Figure 6.** Different Stages of The Lamination Technique

## Test Apparatus

All the beams were tested under the four-point bending in a loading frame of 100 kN capacity. Load at load points and deflection at midspan were measured using mechanical gauges (accuracy 0.01 mm) for incrementally applied loads. Further, crack development, propagation, and mode of failure were also monitored during the process of testing. Figure 7 shows the four- point bending test set up with the beam specimen.

**Figure 7.** Photographic View of The Setup

## RESULTS AND DISCUSSION

### Experimental Results and Discussion

#### *Effect on Strength and Deflection*

The load-carrying capacity and deflection of the beams at the first crack, yield, and ultimate stages were recorded during the experiment and are presented in Table 3. Yield and ultimate loads were determined based on the stage where the load-deflection response became nonlinear, and the beam could no longer sustain additional deformation at the same load intensity.

Table 3 indicates that the first crack load of the laminated RC beam was twice that of the unstrengthened RC beam. Laminated beams exhibited significantly higher yield loads than both BFRC and RC beams, with the laminated BFRC beam showing a 48% increase in yield load due to its improved tensile capacity. The ultimate load capacity increased by 62% for the GFRP-laminated BFRC beam and by 55% for the GFRP-laminated RC beam compared to the RC beam, demonstrating the superior stiffness of the GFRP laminate (Figure 8).

Regarding deflection, the BFRC beam exhibited higher deflection than the RC beam, with increases of 76%, 15%, and 35% at the first crack, yield, and ultimate stages, respectively. This highlights the improved flexibility of RC beams with fibre addition. In contrast, laminated beams showed the greatest reduction in deflection, with a decrease of 39% compared to the RC beam and 147% compared to the BFRC beam (Figure 9).

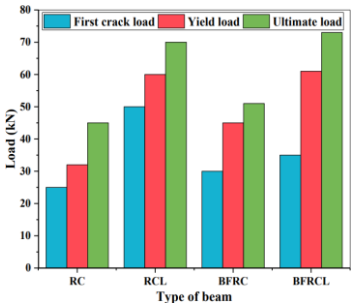


**Figure 8.** Load Carrying Capacity of Beams

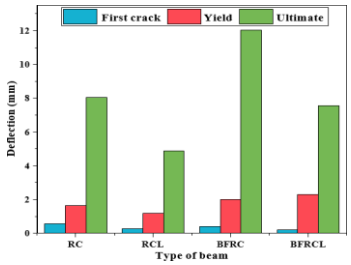


**Figure 9.** Deflection Capacity of Beams

**Table 3.** Summary of the Experimental Results

| Beam ID | First crack stage | | Yield stage | | Ultimate stage | |
|---|---|---|---|---|---|---|
| | Load (kN) | Deflection (mm) | Load (kN) | Deflection (mm) | Load (kN) | Deflection (mm) |
| RC | 25.00 | 0.55 | 32.00 | 1.63 | 45.00 | 8.03 |
| RCL | 50.00 | 0.25 | 60.00 | 1.18 | 70.00 | 12.02 |
| BFRC | 30.00 | 0.38 | 45.00 | 1.98 | 51.00 | 4.86 |
| BFRCL | 35.00 | 0.19 | 61.00 | 2.28 | 73.00 | 7.56 |

### Load-deflection Response

Load-deflection curves are a standardized method of quantifying the energy, which a beam absorbs during its load-induced flexural deflection. The area under the curve represents the energy absorbed by the beam. These curves were drawn using the data obtained from the static flexure test. A significant difference in the behaviour of all the beams is found in the flexure test. When the beams were loaded in flexure, two stages of behaviour have been observed in the load-deflection curve. Load-deflection response of beams is shown in Figure 10. These curves show a linear

variation in the initial stages of loading and then curves are significantly non-linear and reach their peak at the ultimate load or the maximum sustainable load. An overall evaluation of the flexural test results indicates the laminated BFRC beams exhibit higher load carrying capacity.

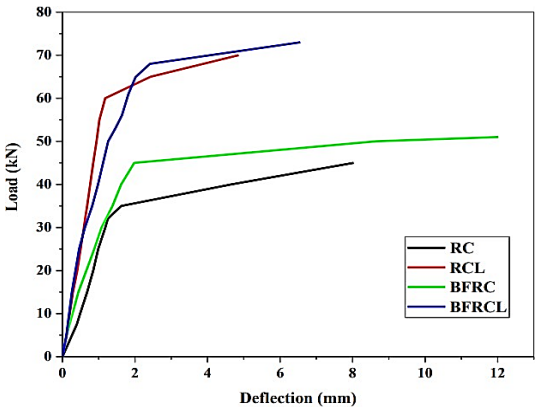


**Figure 10.** Load-deflection Response of Beam Specimens

## Failure Modes

The failure modes of beam specimens are shown in Figure 11. In this study, all the beams failed in flexure mode only. It was noticed that the laminated beams failed due to delamination. In addition, for beams with fibre, the failure was not sudden. The randomly oriented fibres crossing the cracked section resisted the propagation of cracks and separation of the section. It indicates that BFRC effectively relieves expansion of cracks, and the bridging effect of basalt fibre controls the number of cracks and its depth and inhibits the generation and development of cracks.

(a) RC


(b) RCL

(c) BFRC

(d) BFRCL

**Figure 11.** Failure modes of Beam Specimen

## Ductility Index

The ductility of reinforced beams is essentially a measure of their energy absorption capacity. The ductility of a beam is its ability to inelastic deformation without any loss in its load carrying capacity, before failure. Ductility can be expressed in terms of energy or deformation. The deformation can be deflection, strain, or curvature. The load-deflection curves reveal that the addition of fibres influences the overall structural ductility of the beams. To quantify ductility, its indices are calculated in terms of energy, and deflection is presented in Table 7.

It can be inferred from Table 4, that the BFRC beam exhibits enhanced ductility when compared to that of the reference beam. The maximum increase in energy and deflection ductility was found to be up to 1.14 times and 1.23 times, respectively when compared to that of the reference beam. Incidentally, all laminated beams exhibit lower ductility (amongst the beams tested). This phenomenon is on expected lines, as lamination reduces the deflection and hence exhibits lower ductility. The enhancement in energy and deflection ductility for beams is shown in Figure 12.

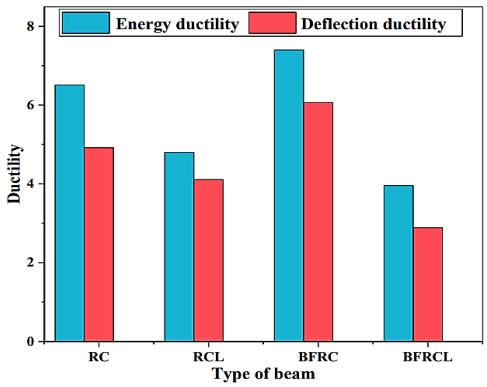


**Figure 12.** Ductility Behaviour of Beams

**Table 4.** Ductility Indices of Beams

| Sl. No. | Beam Specification | Energy Absorption capacity | Energy Ductility Ratio | Deflection Ductility | Deflection Ductility Ratio |
|---|---|---|---|---|---|
| 1 | RC | 6.51 | 1.00 | 4.92 | 1.00 |
| 2 | RCL | 4.80 | 0.74 | 4.11 | 0.84 |
| 3 | BFRC | 7.40 | 1.14 | 6.07 | 1.24 |
| 4 | BFRCL | 3.96 | 0.60 | 2.89 | 0.59 |

## The Numerical Simulation

FE analysis software ANSYS [15] is used to model RC, BFRC, and laminated beams. In the following sections, modelling of beam has been described. This model was specifically employed to accurately trace the response of fibre reinforced and laminated beams by incorporating simulation techniques including nonlinear material properties such as concrete cracking and crushing and yielding of embedded steel reinforcement.

For modelling concrete, the Solid65 3D (Figure 13) element is used, which can represent solids with or without reinforcing bars (rebar). It is defined by eight nodes, each having three degrees of freedom (translations in the x, y, and z directions) and accounts for non-linear material properties. Steel reinforcement is modelled using the Link180 element (Figure 14), a uniaxial tension-compression element with similar degrees of freedom, incorporating plasticity, creep, rotation, large deflection, and large strain capabilities. The steel plates at the supports are represented by the Solid185 (Figure 15) homogeneous structural solid element, which also has eight nodes with three degrees of freedom per node and supports plasticity, hyper-elasticity, stress stiffening, creep, large deflections, and large strains.

Solid185 (Layered Structural Solid) element was used for modelling the GFRP laminates [17]. It is defined by eight nodes having three degrees of freedom at each node: translations in the nodal x, y, and z directions. It has mixed formulation capability for simulating deformations of nearly incompressible elastoplastic materials, and fully incompressible hyper-elastic materials. The element was used to model layered thick shells or solids. The element may be stacked for modelling composites with more than 250 layers or for improving solution accuracy. The geometry of the element is shown Figure 16. On the other hand, materials with orthotropic properties can be assigned to this element, where they can have different properties in each direction, which thus makes them suitable to model

FRP laminates. All FRP sheets were modelled with a laminate thickness of 5 mm. The properties of the GFRP material used for analysis are as follows: The elastic modulus in the x-direction (Ex) is 1603.60 MPa, while in the y- and z-directions (Ey = Ez), it is 217.58 MPa. The Poisson's ratio in the xz-plane (υxz) is 0.38, and in the yz-plane (υyz) is 0.50, which describe how the material deforms in different directions when stretched or compressed. The shear modulus, which measures the material's resistance to shearing forces, is 114.78 MPa in the xy- and xz-planes (Gxy = Gxz) and 72.53 MPa in the yz-plane (Gyz). These properties determine how the GFRP laminate behaves under different loads.

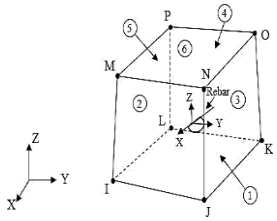


**Figure 13.** Solid65 Element (Concrete)

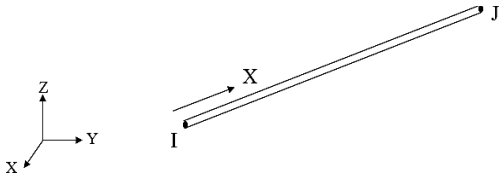


**Figure 14.** Link180 Element (Steel Rebar)

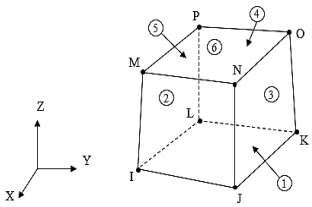


**Figure 15.** Solid185 Element (Steel Plate)

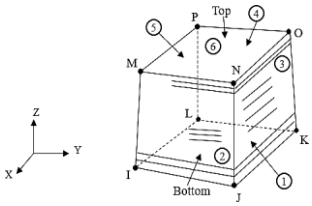


**Figure 16.** Solid185 - Layered Structural Solid Element

### *Modelling Procedure*

Full-scale beams and the reinforcement details was modelled, with the same dimensions used in experimental investigations as shown in Figure 17a & b, respectively. To simulate the strengthening process in the FE, the GFRP layer was modelled as volume and it was attached with the concrete beam (Solid65) block by using Glue command in order to satisfy the perfect bonding condition. Glue is similar to overlap, except that it applies only to cases in which the intersection between entities occurs at a boundary, and is one dimension lower than the original entities. 'The entities maintain their individuality (they are not added), but they become connected at their intersection Figure 17 [18].

After developing the models of beams with supporting plates, it has to be meshed before carrying out the process of analysis. Mesh Tool which is available in pre-processor helps to establish such factors like: mesh attributes; smart size; size controls; mesh shape, which were used for meshing the solid models. To obtain good results, the use of a square or rectangular mesh has been recommended. Therefore, the mesh shape assigned is of square or rectangular elements with 50 mm size. The overall meshed of beam is shown in Figure 18a. Boundary conditions need to be applied at points where the supports and loadings exist. To simulate simply supported condition, UX, UY and UZ at the nodes of one support were given constant values of zero and only UY at the nodes of another support was given constant values of zero. Then the beam was coupled at loading points (at one third of effective span) in order to eliminate stress concentration at the loading points. Two equal forces (W/2) are applied on the coupled nodes (Figure 18b).

Static type of analysis was selected in the entire study to examine three different behaviour such as: initial cracking of the beam, yielding of the steel reinforcement, and the ultimate strength of the beam. Solution Control command was used for controlling (linear and non-linear) analyses and output of the modeled beam in the software. Small displacement with static was considered in the analysis options. In the Time Control, time at end of load step refers to proposed applied load for the complete FE, for which an appropriate load was given to run the analysis effectively without getting convergence problem.

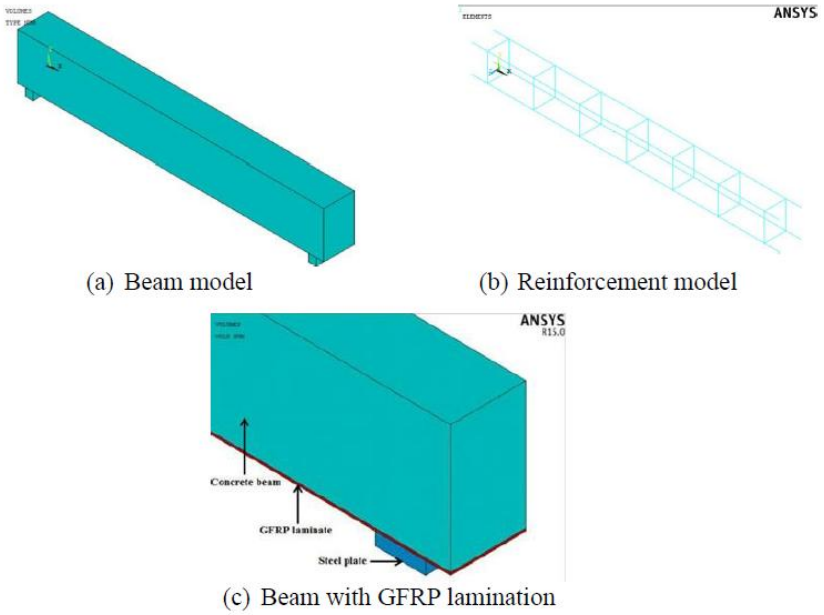


(a) Beam model (b) Reinforcement model

(c) Beam with GFRP lamination

**Figure 17.** Stages in Modelling Procedure

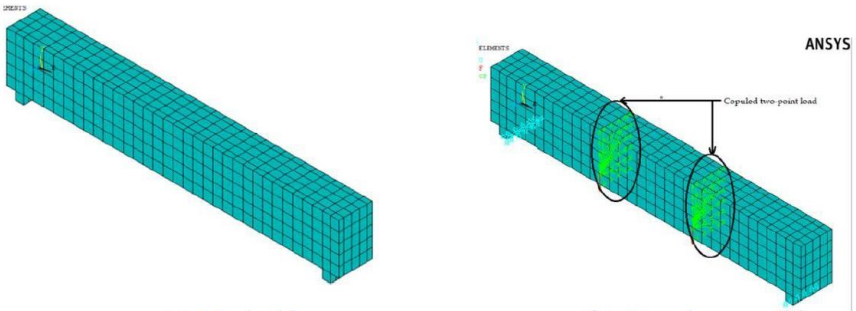


(a) Meshed beam (b) Boundary conditions

**Figure 18.** Mesh and Boundary Conditions of The Modelled Beams

## Validation of Numerical Results

In this section, the adopted numerical procedure is validated by comparing the strength, deflection and load vs midspan deflection response obtained from the numerical analysis against the experimental results.

### *Strength and Deflection*

The load-deflection graphs presented in Figure 19 compares experimental and numerical results for RC, RCL, BFRC, and BFRCL specimens. All exhibit an initial linear response followed by non-linear behaviour, with numerical models slightly overestimating the load due to idealized conditions. Basalt fibres enhance ductility and increase load capacity, while lightweight aggregates slightly reduce stiffness but maintain comparable peak loads. The close agreement between numerical and experimental trends validates the model and highlights the benefits of fibre reinforcement. From Table 5, it can be learned that the difference between the numerical and experimental response of all beams is less than 5%, which in turn depicts the accuracy of the adopted FE non-linear numerical analysis. The overall average value of the *Py, Num.* / *Py, Exp.* ratio for the beams is 1.02 with a standard deviation and coefficient of variation are 0.01 and 1.41%, respectively. In addition, the overall average value of the $\delta y$, *num.* / $\delta y$, *exp.* ratio for the beams is 1.04 with a standard deviation and coefficient of variation are 0.01 and 1.04%, respectively.

From Table 5, it can be learned that the difference between the numerical and experimental response of all beams is less than 5%, which in turn depicts the accuracy of the adopted FE non-linear numerical analysis. The overall average value of the *Pu, num.* / *Pu, exp.* ratio for the beams is 0.96 with a standard deviation and coefficient of variation are 0.01 and 0.79%, respectively. In addition, the overall average value of the *δu, num.* / *δu, exp.* ratio for the beams is 0.99 with a standard deviation and coefficient of variation are 0.03 and 2.89%, respectively.

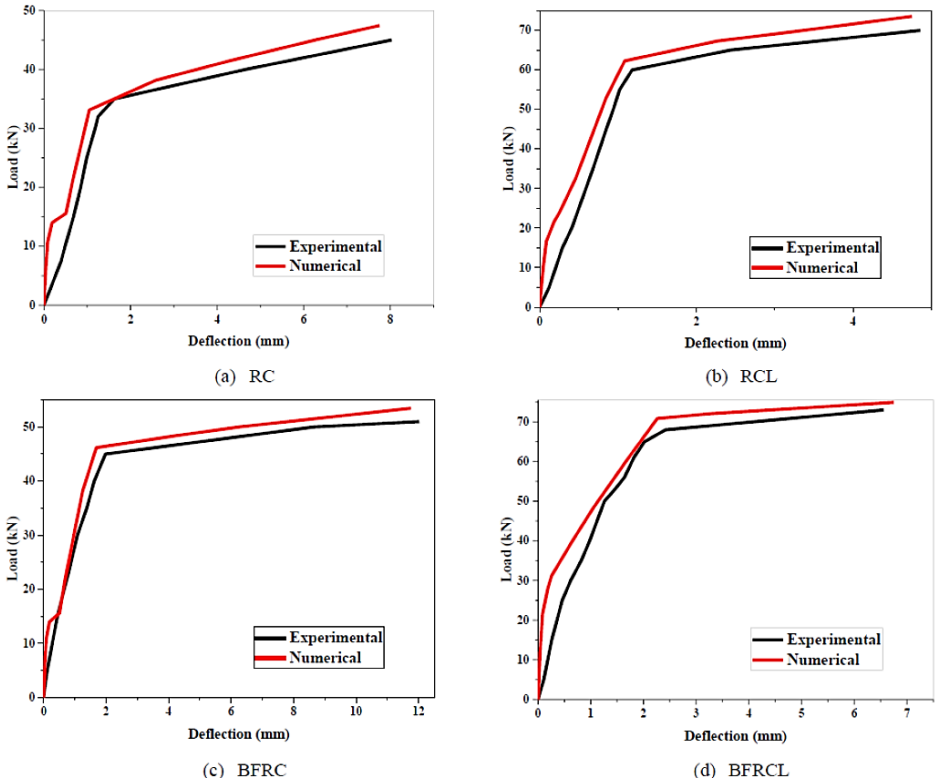


**Figure 19** Load Deflection Responses of Beam Samples

**Table 5.** Comparative Results at Ultimate Stage

| Beam ID | Ultimate load (*Pu*) (kN) | | % | Pu, num. | Deflection (*δu*) (mm) | | % | δu, num./ |
|---|---|---|---|---|---|---|---|---|
| | Pu, exp. | Pu, num. | Difference in load | / Pu, exp. | δu, exp. | δu, num. | difference in deflection | δu, exp. |
| RC | 45.00 | 1.55 | 4.91 | 0.95 | 8.03 | 7.75 | 3.49 | 0.97 |
| RCL | 70.00 | 1.14 | 3.39 | 0.97 | 12.02 | 4.75 | 2.26 | 0.98 |
| BFRC | 51.00 | 1.89 | 4.55 | 0.95 | 4.86 | 11.75 | 2.25 | 0.98 |
| BFRCL | 73.00 | 2.2 | 3.51 | 0.96 | 7.56 | 6.75 | 2.90 | 1.03 |

It is seen that the yield and ultimate load of the beams obtained by the experimental study is consistently and slightly lower than of the numerical study. In addition, the yield and ultimate deflection of all the all beams obtained by the experimental study is consistently and slightly higher than the results from the numerical study. This may be due to the bond-slip between concrete and steel reinforcement, as well as between concrete and the laminate, which is not considered in the numerical model.

## *Crack Pattern*

ANSYS can generate crack propagation for each sub step from the stage of formation of the first crack to the ultimate stage. From Figure 20, it can be understood that the modelled first crack in all the beams was found under the loading points in the extreme tension face of the beam. In the subsequent substeps, the flexural cracks in the beams are developed towards the mid-span and shear span of the beam, and the crack length propagated towards the compression zone of the beams. Then, a few compressive cracks and diagonal tensile cracks were formed near the loading points and in the shear span, respectively, in the beam, at the ultimate stage. Further, the maximum number of flexural cracks and multiple cracks were also formed in the mid-span. The above trend is similar to the observations during experimental investigations. In addition, it is seen from the crack pattern at the ultimate stage of the beams that there may be a possibility of concrete cover separation or debonding of laminate from the concrete surface, due to the excessive concentration of flexural cracks at the extreme tension face of the beam.

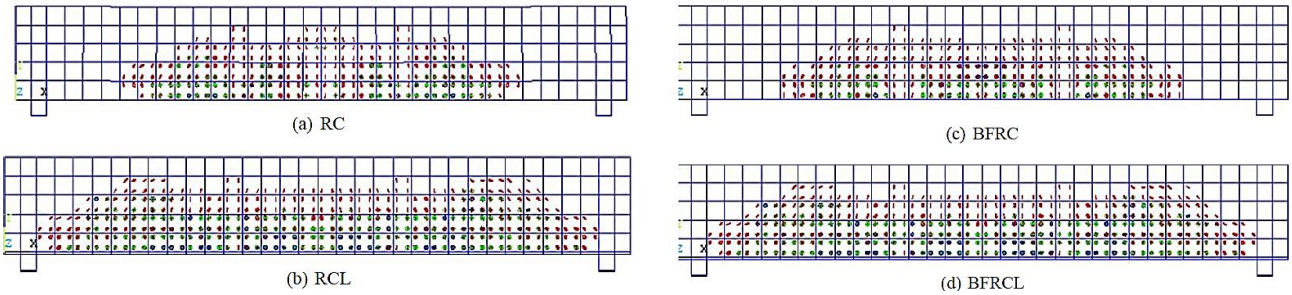


**Figure 20.** Crack Pattern of The Beam Specimens at Ultimate Stage

## CONCLUSIONS

The experimental and numerical analysis of RC, BFRC, and GFRP-laminated beams led to several key conclusions. Among all tested beams, the GFRP-laminated BFRC beam demonstrated the highest load-carrying capacity, with an ultimate load increase of 55% compared to the RC beam and 29% compared to the BFRC beam. The GFRP-laminated RC beam exhibited the greatest reduction in deflection, with a 65% decrease compared to the RC beam and 147% compared to the BFRC beam. However, all laminated beams showed lower ductility, as expected, due to reduced deflection. The BFRC beam without lamination exhibited the highest increase in deflection and energy ductility, with a 15% improvement over the RC beam. All beams failed in flexural mode, with laminated beams experiencing failure due to debonding caused by flexural crack propagation. The experimental results closely matched the numerical findings, with load and deflection differences remaining within 5% at all stages, confirming the accuracy and reliability of the adopted numerical approach.

## ACKNOWLEDGEMENT

The authors wish to acknowledge the Department of Civil Engineering, Pondicherry Engineering College, Puducherry, for providing lab facility to carry out the dissertation project work.

## REFERENCES

1. Al-saawani, M.A., Al-negheimish, A.I., El-sayed, A.K., and Alhozaimy, A.M., Finite Element Modelling of Debonding Failures in FRP-Strengthened Concrete Beams using Cohesive Zone Model, *Polymers (Basel)*, *14*, 2022, pp. 1-23.
2. Rabinovitch, O. and Frostig, Y., Experiments and Analytical Comparison of RC Beams Strengthened with CFRP Composites, *Composites Part B: Engineering*, *34*(8), 2003, pp. 663–677.
3. Feizbahr, M., Jayaprakash, J., Jamshidi, M., and Keogn, C.K., Review on Various Types and Failures of Fibre Reinforcement Polymer, *Middle East Journal of Scientific Research*, *13*(10), 2013, pp. 1312–1318.
4. Syed Ibrahim, S., Eswari, S., and Thirumalai, S., Structural Performance of Glass Fibre Reinforced Polymer Laminated Steel Fibre Reinforced Concrete Beams, *Asian Journal of Civil Enigineering*, *17*(1), 2016, pp. 59–66.
5. Bheel, N. and Basalt Fibre-Reinforced Concrete: Review of Fresh and Mechanical Properties, *Journal of Building Pathology and Rehabilitation, 6*(1), 2021, pp. 1–9.
6. Mahini, S.S. and Ronagh, H.R., Strength and Ductility of FRP Web-Bonded RC Beams for the Assessment of Retrofitted Beam-Column Joints, *Composite Structures*, *92*(6), 2010, pp. 1325–1332.
7. Galal, K. and Mofidi, A., Strengthening RC Beams in Flexure Using New Hybrid FRP Sheet/Ductile Anchor System, *Journal of Compoite for Construction*, *13*(3), 2009, pp. 217–225.
8. Alabduljabbar, H. et al., Mechanical Effect of Steel Fibre on the Cement Replacement Materials of Self-Compacting Concrete, *Fibres*, *7*(4), 2019, pp. 1–11.
9. Jiang, C., Fan, K., Wu, F., and Chen, D., Experimental Study on the Mechanical Properties and Microstructure of Chopped Basalt Fibre Reinforced Concrete, *Materials & Design*, *58*, 2014, pp. 187–193.
10. Mishnaevsky, L. and Dai, G., Hybrid Carbon/glass Fibre Composites: Micromechanical Analysis of Structure-damage Resistance Relationships, *Computational Material Science*, *81*, 2014, pp. 630–640.
11. Deák, T. and Czigány, T., Chemical Composition and Mechanical Properties of Basalt and Glass Fibres: A Comparison, *Textile Research Journal*, *79*(7), 2009, pp. 645–651.
12. Hawileh, R.A. et al., Finite Element Modelling of Reinforced Concrete Beams Externally Strengthened in Flexure with Side-bonded FRP Laminates, *Composites Part B Engineering, 173*(October 2018), 2019, p.

106952.
13. Kachlakev, D. and McCurry, D.D., Behaviour of Full-Scale Reinforced Concrete Beams Retrofitted for Shear and Flexural with FRP Laminates, *Composites Part B Engineering*, *31*(6–7), 2000, pp. 445–452.
14. Chiew, S.-P. et al., Flexural Strength of RC Beams with GFRP Laminates, *Journal of Composites for Construction*, *11*(5), 2007, pp. 497–506.
15. ANSYS: *A Finite Element Computer Software and User Manual for Nonlinear Structural Analysis*, Canonsburg, 2007.
16. Li, Y.F. et al., Effect of the Sizing Removal Methods of Fibre Surface on the Mechanical Performance of Basalt Fibre-Reinforced Concrete, *Fibres*, *12*(1), 2024.
17. Syed Ibrahim, S. et al., Effect of Discrete Steel Fibres on Strength and Ductility of FRP Laminated RC Beams, *Ain Shams Engineering Journal*, *12*(2), 2021, pp. 1329–1337.
18. Miller, T.H. et al., FE Models of GFRP and CFRP Strengthening of Reinforced Concrete Beams, *Advances in Civil Engineering*, 2009.